ACS Energy LETTERS

http://pubs.acs.org/journal/aelccp

Defect Tolerance of Mixed B-Site Organic–Inorganic Halide Perovskites

Jian Xu,[†] Aidan Maxwell,[†] Mingyang Wei, Zaiwei Wang, Bin Chen, Tong Zhu, and Edward H. Sargent*

Cite This: *ACS Energy Lett.* 2021, 6, 4220–4227

Read Online

ACCESS | Metrics & More | Article Recommendations | Supporting Information

ABSTRACT: Further improvements in the photovoltaic performance of B-site alloyed organic–inorganic halide perovskites (OIHPs) will rely on accurate modeling of defect properties and passivation strategies. Herein, we report that B-site alloying results in defect behaviors distinct from those of pure OIHPs, a finding obtained by uniting first-principles calculations with experimental measurements. We identify from computational studies a defect-tolerant region spanning a Sn content of 30–70% in mixed Pb-Sn perovskites and experimentally observe notably longer carrier lifetimes in 50% Sn mixed perovskite films than at other Sn contents. We discuss a strategy of applying defect-tolerant 50% Pb-Sn perovskites in ideal-bandgap (1.3–1.4 eV) active layer materials which conventionally rely on 25–30% Sn compositions. The composition ($FA_{0.75}Cs_{0.25}Pb_{0.5}Sn_{0.5}(I_{0.9}Br_{0.1})_3$) achieves increased carrier lifetimes of >1 μs. This work reveals a general trend in defect tolerance for B-site alloying: a higher valence band maximum (lower conduction band minimum), along with strengthened ionic bonding, can potentially contribute to improved photovoltaic performance.

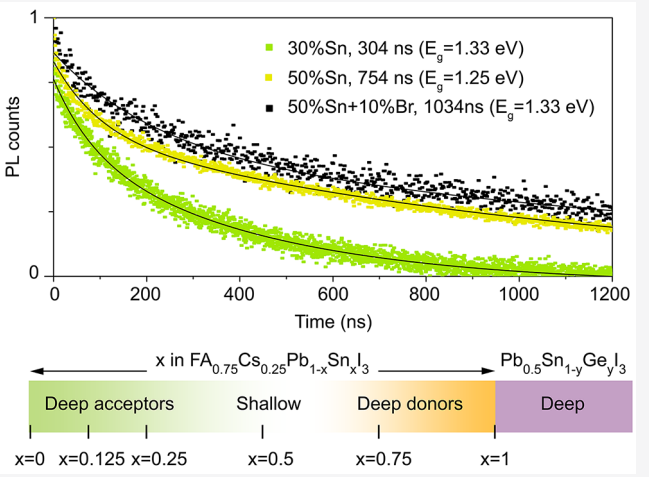

Lead-based organic–inorganic halide perovskites (OIHPs) are attractive light-absorber materials for photovoltaic (PV) applications, as seen by their rapid increase in power conversion efficiency (PCE) to 25.5%.[1] Compositional engineering at the B-site with Sn^{2+} and Ge^{2+} is an important strategy to regulate optoelectronic properties and to ease regulatory constraints related to the use of toxic Pb. B-site alloying can also provide a bandgap (E_g) as low as ~1.2 eV in mixed Pb-Sn OIHPs relevant to all-perovskite tandems that offer routes to go beyond the Shockley–Queisser limit of single-junction solar cells.[2−4] The record certified efficiency of all-perovskite tandems has reached 26.4%, comparable to that of the best-performing silicon solar cells.[5] One remaining area for significant further improvement is the development of efficient narrow-E_g perovskites as the bottom subcell.[6−8]

The ideal E_g for the maximum PCE of single-junction solar cells is 1.3–1.4 eV.[9] In order to reach this E_g, it is generally necessary to use 25–30% Sn content in mixed Pb-Sn perovskites,[10,11] resulting in PCEs that lag behind those of narrow-E_g (~1.2 eV) Pb-Sn solar cells. The lagging efficiency of ideal-E_g Pb-Sn solar cells arises from high defect densities, which limits carrier lifetimes. Zhou et al. reported carrier lifetime values of 156 and 821 ns for $MA_{0.3}FA_{0.7}Pb_{0.7}Sn_{0.3}I_3$ perovskite films without and with 12% Br.[10] Yang et al. reported a promising 50% Sn composition ($MAPb_{0.5}Sn_{0.5}(I_{0.8}Br_{0.2})_3$) for ideal-$E_g$ devices,[11] a finding that motivates further study of materials in this composition.

Recent experimental work has investigated the PV performance of mixed Pb-Sn perovskites and identified a concentration range of heavy defectivity at a low Sn content of 0.5–20%.[12] This phenomenon is intriguing, especially given that the problems traceable to Sn oxidation are expected to rise with higher Sn concentration.[13] We undertook, with this in mind, a study of how B-site alloying impacts the defect properties of OIHPs.

Defect properties influence carrier density, carrier lifetime, and transport properties in semiconductors.[14] Defect physics in pure OIHPs has been studied extensively; fewer studies focus on B-site alloyed systems.[15−21] We note also the

Received: September 27, 2021
Accepted: November 2, 2021

https://doi.org/10.1021/acsenergylett.1c02105
ACS Energy Lett. 2021, 6, 4220–4227

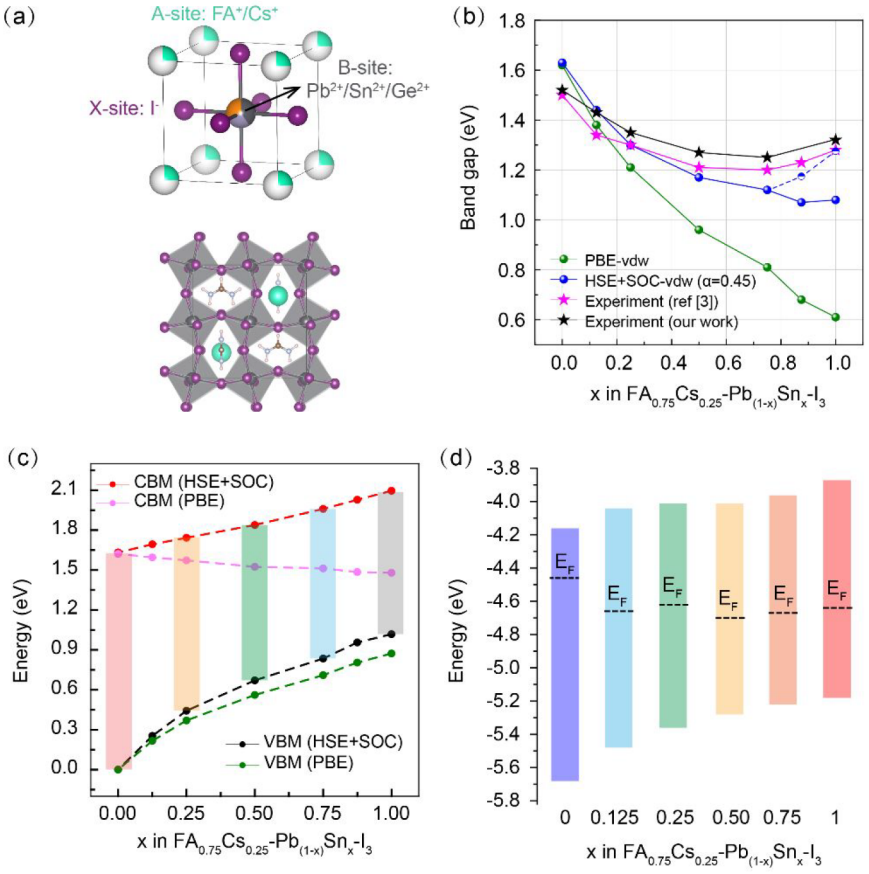

Figure 1. (a) Atomic structure of ABX_3 and $FA_{0.75}Cs_{0.25}PbI_3$. (b) Calculated and experimental bandgap values in $FA_{0.75}Cs_{0.25}Pb_{(1-x)}Sn_xI_3$ measured using UV-vis-NIR absorption spectroscopy. (c) Calculated band edge positions comparing PBE and HSE+SOC methods in $FA_{0.75}Cs_{0.25}Pb_{1-x}Sn_xI_3$. (d) Band alignment of $FA_{0.75}Cs_{0.25}Pb_{1-x}Sn_xI_3$ determined from UPS and UV-vis-NIR measurements.

limitations of the Perdew−Burke−Ernzerhof (PBE) method, which can lead even to incorrect trends, such as that shallow traps dominate in bulk OIHPs[15,16]—computational studies whose trends diverge with those from experiments.[22−24] We therefore used hybrid functionals including a spin−orbital coupling (HSE+SOC) method to examine the defect properties.[25−28]

Combining computational and experimental efforts, we investigated defect properties in B-site alloyed OIHPs. We find that the HSE+SOC calculation method gives band edge trends that agree with experiments. We then identify a region (30−70% Sn content) of defect tolerance in mixed Pb-Sn perovskites, with 50% Sn mixed perovskite exhibiting notably longer carrier lifetimes than all other Sn contents. Using a defect-tolerant 50% Sn composition with 10% Br ($FA_{0.75}Cs_{0.25}Pb_{0.5}Sn_{0.5}(I_{0.9}Br_{0.1})_3$), we then demonstrate perovskite thin films with the same ideal E_g (1.33 eV) as conventional 30% Sn compositions, and we observe a significantly increased carrier lifetime from 304 to 1034 ns, comparable to the longest values reported to date for MA-free Pb-Sn perovskites. Our calculations also indicate the potential of alloying alkaline earth metals to improve the PV performance of Pb-Sn perovskites.

The mixed A-site composition of $FA_{0.75}Cs_{0.25}$ in perovskites has been reported to have enhanced stability due to improved resistance to moisture and oxidation.[29,30] Thus, we chose $FA_{0.75}Cs_{0.25}BI_3$ (B = Pb^{2+}, Sn^{2+}, Ge^{2+}) for investigation in this work (Figure 1a). Pb-Sn alloyed systems were thermodynamically more favorable than the pure Pb and pure Sn at 300 K (Figure S3). As shown in Figure 1b, we observed the expected E_g bowing character with the minimum values (~1.2 eV) found in the range of 50−75% Sn in $FA_{0.75}Cs_{0.25}Pb_{(1-x)}Sn_xI_3$, which can be explained by the electronic structures (Note 2 in the Supporting Information and Figure S4). It is well known that the HSE+SOC method gives E_g values more consistent with experiments than the PBE method. However, few reports discuss whether HSE+SOC band edge position predictions are consistent with experiments. Thus, we performed UV-vis-NIR absorption spectroscopy and ultraviolet photoemission spectroscopy (UPS) measurements of $FA_{0.75}Cs_{0.25}Pb_{1-x}Sn_xI_3$ thin films (Figure 1d and Figure S1). We observed an upshift of the valence band maximum (VBM) and conduction band minimum (CBM) with increasing Sn content, consistent with our HSE+SOC calculations (Figure 1c). We noted that the experimental VBM/CBM energy shifts are more limited compared to the calculated ones, potentially due to the antioxidant additive incorporation and imperfections of the perovskite surface in experiment and because UPS is a surface-sensitive probing technique.[31]

To investigate the effect of B-site alloying on the defect properties of OIHPs, we performed defect calculations in a large 4×4×4 supercell (656 atoms) using the HSE+SOC method. Charge-state transition levels (CTLs)[32] are commonly used as a criterion to identify point defects as shallow or deep (see Methods section in the Supporting Information). We emphasize the importance of accurate predictions of band

https://doi.org/10.1021/acsenergylett.1c02105
ACS Energy Lett. 2021, 6, 4220−4227

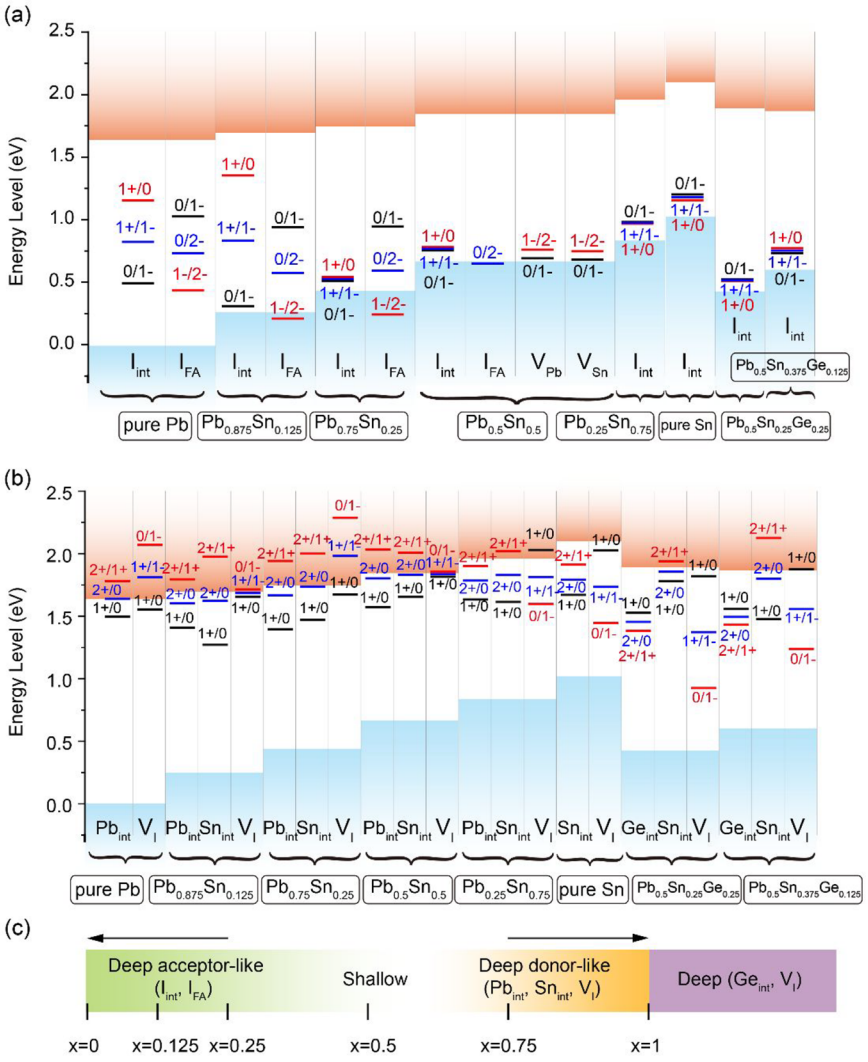

Figure 2. Calculated charge-state transition levels (CTLs) for intrinsic (a) acceptor-like defects and (b) donor-like defects in $FA_{0.75}Cs_{0.25}Pb_{(1-x)}Sn_xI_3$ and $FA_{0.75}Cs_{0.25}Pb_{0.5}Sn_{(1-y)}Ge_yI_3$. The CTL values (in eV) of alloys were referenced to the host VBM of pure Pb. (c) Schematic diagram of the defect tolerance behaviors in mixed Pb-Sn and mixed Pb-Sn-Ge alloys.

edge position on the correct evaluation of CTLs and defect formation energies. HSE+SOC predictions resulted in a downshift of both the VBM an CBM relative to the PBE results. As shown in Figure S5, we found that PBE-predicted shallow acceptors (deep donors) may become deep trap states (shallow states) in the HSE+SOC calculations (e.g., iodine interstitial (I_{int}) for the former; Sn/Pb interstitial (Sn_{int}/Pb_{int}) and iodine vacancy (V_I) for the latter). These results are qualitatively consistent with previous work investigating $MAPbI_3$.[25−27]

Figure 2 shows the calculated CTLs for defects in B-site alloyed perovskites. For mixed Pb-Sn perovskites, we find that the CTLs are mainly modulated by band edge positions, while their absolute values are less sensitive to the Sn content. Importantly, the 50% Sn mixed alloy exhibits enhanced defect tolerance and is free of deep traps. Some deep acceptors in pure Pb (e.g., I_{int}, I_{FA}) with a lower VBM become shallower in 30−70% Sn mixed alloys. We also examine the defect levels of Sn vacancies (V_{Sn}) in 30% and 50% Sn mixed systems and find that V_{Sn} are shallow defects in these compositions (Figure S6). Analogously, some deep donors in pure Sn (e.g., Sn_{int}, V_I) with a higher CBM also become shallower in 30−70% Sn mixed alloys. Additional discussion of the defect properties in literature is in Note 3 in the Supporting Information.

We then explored, now going beyond defect properties alone, the degradation feasibility of alloys in the presence of oxygen. Along two possible degradation pathways (eqs 1 and 2),[13,33]

$$2APb_{(1-x)}Sn_xI_3 + 2xO_2 \rightarrow 2(1-x)PbI_2 + 2xSnO_2 + 2xI_2 + 2AI \quad (1)$$

$$4CH(NH_2)_2Pb_{(1-x)}Sn_xI_3 + O_2 \rightarrow 4(1-x)PbI_2 + 4xSnI_2 + 2I_2 + 2H_2O + 4CH_4N_2 \quad (2)$$

we calculated the reaction energies, defined as the energy difference between the reactants and products, as a function of the Sn content. From Figure S7, we found that reaction energy increased with Sn content, indicating increased energetic favorability of oxidation. This was also observed in previous experimental work.[13]

https://doi.org/10.1021/acsenergylett.1c02105
ACS Energy Lett. 2021, 6, 4220−4227

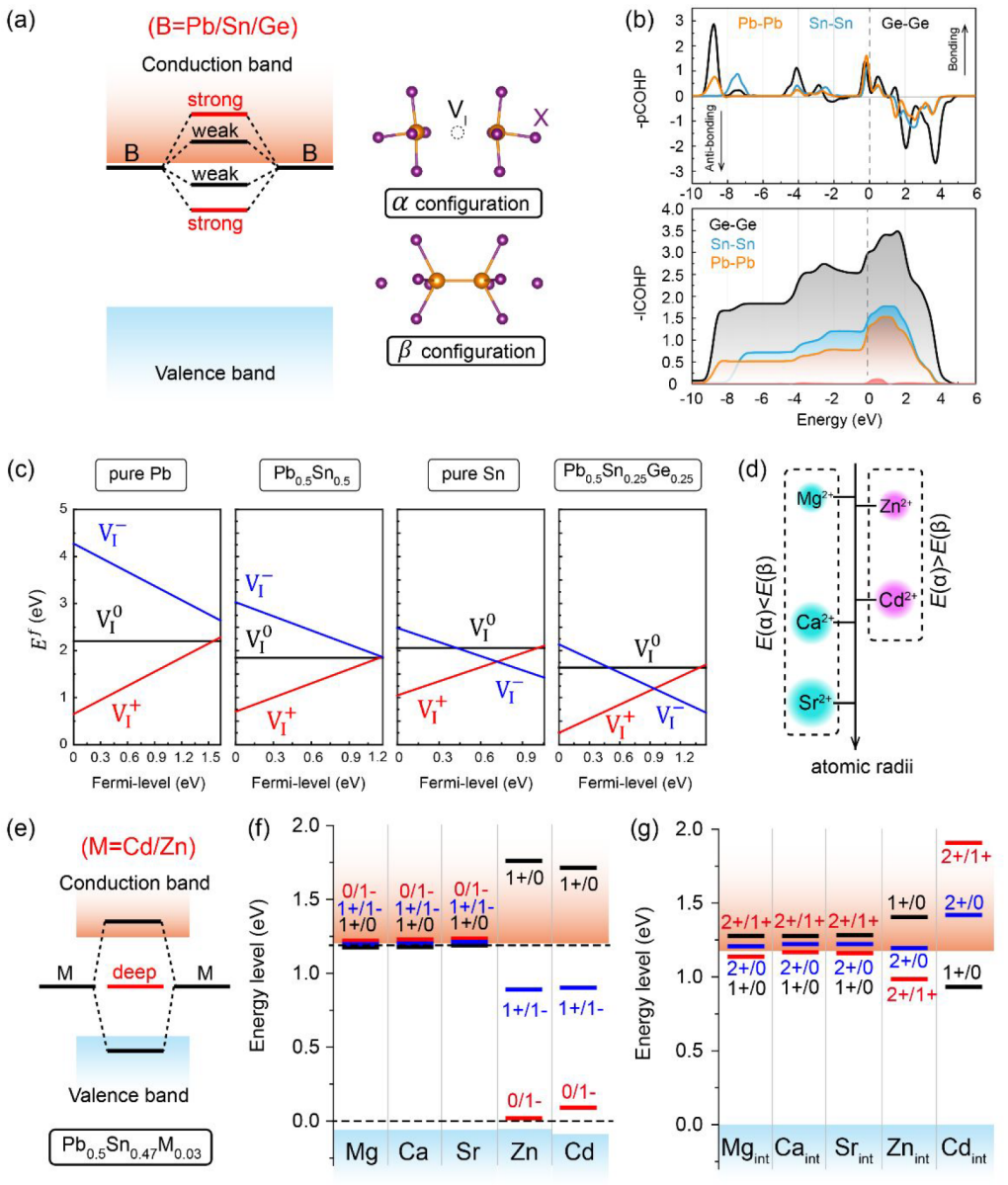

Figure 3. (a) Effect of orbital hybridization strength on the formation of defect levels for V_I^-. The local structures of α and β configurations for V_I^- are also shown. (b) COHP and ICOHP analysis for B−B bonding (B = Pb/Sn/Ge). (c) Calculated formation energies of V_I with different charge states (0, 1+, and 1−) in pure Pb, pure Sn, $Pb_{0.5}Sn_{0.5}$, and $Pb_{0.5}Sn_{0.25}Ge_{0.25}$ under I-medium conditions, as a function of the Fermi level. The Fermi levels were referenced to their host VBM. (d) B-site candidates for incorporation. (e) Schematic demonstrating the orbital hybridization for V_I^- in $Pb_{0.5}Sn_{0.47}M_{0.03}$ (M = Zn^{2+}, Cd^{2+}). (f) CTLs of V_I in $Pb_{0.5}Sn_{0.47}M_{0.03}$ (M = Mg^{2+}, Ca^{2+}, Sr^{2+}, Zn^{2+}, Cd^{2+}), referenced to the host VBM of $Pb_{0.5}Sn_{0.5}$. (g) CTLs of M_{int} in $Pb_{0.5}Sn_{0.5}$.

Taking account of bulk defect properties along with the increased susceptibility to Sn oxidation with Sn alloying, we expected 30−70% Sn mixed perovskite films to exhibit enhanced defect tolerance. For Sn contents <30%, deep-level acceptors were expected to result in heavier defectiveness and nonradiative recombination. Taking 12.5% Sn mixed perovskite for instance, I_{int} induced an $\varepsilon(1-/1+)$ CTL deep within the bandgap (0.57 eV above the VBM). However, I_{int} behaved differently in 50% Sn mixed perovskite, with both $\varepsilon(0/1+)$ and $\varepsilon(0/1-)$ near the VBM, acting as a shallow defect. For Sn contents >75%, the optoelectronic properties were expected to be limited by the deep-level donors, increased oxidation of Sn^{2+}, and the subsequent heavy hole-doping.

We further investigated the effect of alloying Ge into mixed Pb-Sn perovskites on defect properties, to look for a more general trend in the defect tolerance in B-site alloyed OIHPs. Here we focus on V_I, an important defect in perovskites.[34] To reduce the oxidation of Sn^{2+}/Ge^{2+}, we prefer to create a Sn(Ge)-rich/I-poor condition, which will promote the formation of V_I. For negatively charged V_I^-, there exist two possible configurations (α and β), as shown in Figure 3a. The formation of the localized β state was determined by the competition between the energy-gain obtained by moving the electrons from the α state to the β state (ΔE_{el}) and the energy-loss from atomic distortion (ΔE_{st}).[19] Taking $Pb_{0.5}Sn_{0.25}Ge_{0.25}$ for instance, the $\varepsilon(1+/1-)$ CTL of V_I is located at 0.51 eV below the CBM, indicating the dominant presence of V_I^+ (V_I^-)

https://doi.org/10.1021/acsenergylett.1c02105
ACS Energy Lett. 2021, 6, 4220−4227

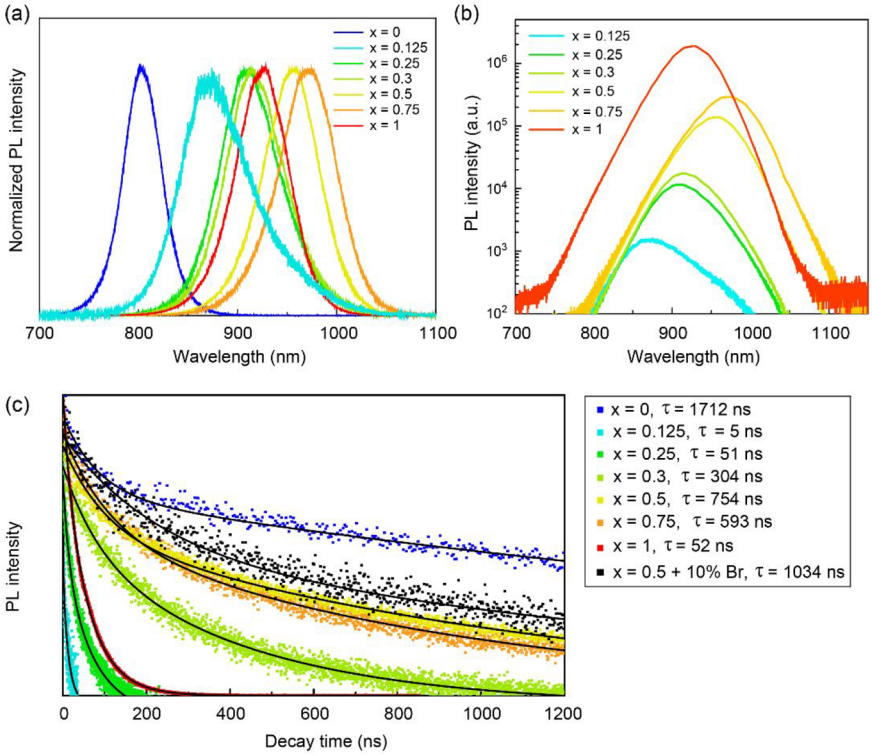

Figure 4. (a) Normalized steady-state photoluminescence (PL) spectra, (b) absolute PL emission intensities, and (c) time-resolved PL spectra of $FA_{0.75}Cs_{0.25}Pb_{(1-x)}Sn_xI_3$ perovskite films.

below (above) this CTL point. This behavior of V_I, i.e., the conversion of a shallow donor into a deep acceptor when the Fermi level approaches the CBM, is called a DX center in some tetrahedral semiconductors.[35−37]

The behavior of V_I in B-site alloyed OIHPs—shallow in pure Pb and 50% mixed Pb-Sn perovskite while deep in pure Sn and the Pb-Sn-Ge alloy—we attribute to the following properties. First, the higher CBM in pure Sn causes much higher ΔE_{el}; thus $\Delta E_{el} > \Delta E_{st}$. This results in the stabilization of the deep β state ($E_\alpha > E_\beta$) and the localized $\varepsilon(1+/1-)$ CTL deep within the bandgap. However, in pure Pb and the $Pb_{0.5}Sn_{0.5}$ alloy, the energy-gain may not be sufficient to overcome the energy-loss, resulting in very similar energies for the α and β configurations, within 0.02 eV ($E_\alpha \approx E_\beta$). The Δ ($\Delta = E_\beta - E_\alpha$) values of these compositions are listed in Table S1. Therefore, V_I in pure Pb and $Pb_{0.5}Sn_{0.5}$ behave as shallow defects, as shown in Figure 2b.

Second, we assign a role to B−B covalent bonding strength. From Figure 3b, the defect levels in the β configuration were derived from the B−B bonding state, and the Ge−Ge covalent bonding was much stronger than the Sn−Sn and Pb−Pb bonding. We attribute this to the smaller ionic radii of Ge^{2+} (0.73 Å) compared with Sn^{2+} (1.05 Å) and Pb^{2+} (1.19 Å). As illustrated in Figure 3a, stronger B−B bonding results in deeper defect states with respect to the CBM. Though $Pb_{0.5}Sn_{0.5}$ and $Pb_{0.5}Sn_{0.25}Ge_{0.25}$ were predicted to have similar CBM positions, V_I had a much deeper $\varepsilon(1+/1-)$ CTL for $Pb_{0.5}Sn_{0.25}Ge_{0.25}$ than $Pb_{0.5}Sn_{0.5}$, as well as a much lower formation energy (Figure 3c).

In addition, we examine the effect of doping extrinsic metals into mixed Pb-Sn perovskite ($Pb_{0.5}Sn_{0.47}M_{0.03}$) on the CTL of V_I. We find that V_I^- is stable in the α configuration ($E_\alpha < E_\beta$) in perovskites doped with alkaline earth metals (M = Mg^{2+}, Ca^{2+}, Sr^{2+}), while they are stable in the β configuration ($E_\alpha > E_\beta$) with doping of transition metals (M = Zn^{2+}, Cd^{2+}), as shown in Figure 3d. The stronger M−M or B−M bonding near the V_I site in the Zn^{2+}/Cd^{2+}-doped system results in higher ΔE_{el} energy gain; thus the β configuration will have a lower energy than the α configuration. From Figure 3e,f, we find that doping M = Mg^{2+}, Ca^{2+}, Sr^{2+} with the outermost electron configuration of s^0d^0 does not create deep states for V_I, in contrast to M = Zn^{2+}, Cd^{2+} with the outermost electron configuration of s^0d^{10}. Interestingly, this trend has little dependence on the atomic radii. As shown in Figure S8, we also check the CTLs of V_I in Zn^{2+}/Cd^{2+}-doped perovskites with a lower doping concentration of 1.5% ($Pb_{0.5}Sn_{0.485}M_{0.015}$) and find that V_I remains deep within the bandgap. The atomic positions of the V_I in doped systems are depicted in Figure S9. From Figure 3f, we can see that dopant incorporation induces a VBM downshift (0.05−0.08 eV) compared with the VBM of non-doped perovskites, which is beneficial in alleviating the detrimental hole-doping of Pb-Sn perovskites.[38] In addition, Phung et al. found that incorporation of Mg^{2+} and Sr^{2+} could increase the formation energy of Pb vacancies (V_{Pb}), indicating the defect density reduction of V_{Pb}.[39] We offer that doping alkaline earth metals has the potential to improve PV performance in Pb-Sn perovskites.[39,40]

We checked for the classification of defects as deep vs shallow, looking at the localized/delocalized wavefunction in the neutral charge state.[41−43] Though B_{int}^0 induced localized defect states inside the bandgap, the large atomic relaxation near B_{int}^{2+} from strong Coulomb interactions may cause a large reduction in its formation energy, resulting in negative-U behavior (Figure S10).[44] Importantly, we found that the stronger B−X ionic bonding strength induced a higher unoccupied energy level in B_{int}^{2+} with respect to the CBM,

https://doi.org/10.1021/acsenergylett.1c02105
ACS Energy Lett. 2021, 6, 4220−4227

resulting in a shallower defect CTL. As shown in Figures 2b and 3g, Ge_{int} and Zn_{int} create deep states within the bandgap, while other B-site interstitials (Mg^{2+}, Ca^{2+}, Sr^{2+}, Cd^{2+}) are shallow.

Overall, we find that the band edge positions and coordination environment (short-range orbital hybridization and long-range electrostatic interaction) determine the defect properties in B-site alloyed systems. We conclude two general trends of enhanced defect tolerance in OIHPs via B-site alloying: (i) A higher VBM (lower CBM) is beneficial for the suppression of deep acceptors (donors). (ii) Stronger B−X ionic bonding and weaker B−B covalent bonding yield shallower defects.

Finally, we carried out experimental measurements to explore further the property of defect tolerance. We observed a decrease in PCE of mixed Pb-Sn perovskite solar cells when alloying Ge at the B-site (Table S2). We then turned our focus to measuring the optoelectronic properties of mixed Pb-Sn perovskites with varying Sn content. We first performed steady-state photoluminescence (PL) measurements on $FA_{0.75}Cs_{0.25}Pb_{(1-x)}Sn_xI_3$ perovskite films. As shown in Figure 4a, the general trend of PL peak shifts agrees well with the optical E_g of the films measured using UV-vis-NIR spectroscopy (Figure S1). Interestingly, we found that the PL intensities were enhanced noticeably for Sn contents of 50% or higher (Figure 4b). We then employed time-resolved photoluminescence (TRPL) to study the carrier dynamics of the Pb-Sn perovskites. As shown in Figure 4c, both Sn-poor (<30%) and Sn-rich (>75%) mixed Pb-Sn perovskites exhibited much shorter PL lifetimes, indicative of their highly defective nature. However, the carrier lifetimes were significantly improved to 754 ns at 50% Sn, implying suppressed non-radiative recombination.

Since 50% Sn mixed perovskites are significantly more defect tolerant, as we have shown theoretically and experimentally, we sought to determine whether the defect-tolerant nature of 50% Sn mixed Pb-Sn perovskites could be applied beyond narrow-E_g perovskites to ideal-E_g single-junction solar cells. Using a 10% Br composition of $FA_{0.75}Cs_{0.25}Pb_{0.5}Sn_{0.5}(I_{0.9}Br_{0.1})_3$, we achieved the same ideal E_g as with Br-free 30% Sn thin films (1.33 eV) and observed a significantly increased carrier lifetime from 304 to 1034 ns (Figure 4c and Figure S11), among the longest carrier lifetimes reported for MA-free Pb-Sn perovskites. This can be partly attributed to the stronger B−X (X = Br) bonding than when X = I.[19] Our calculations also confirm that both I_{int} and Br_{int} are shallow defects in this composition (Figure S12).

In summary, we have combined advanced first-principles defect calculations, UV-vis-NIR, UPS, steady-state PL, and TRPL measurements to investigate the effects of B-site alloying on the optoelectronic properties of OIHPs. We identified a region of enhanced defect tolerance spanning Sn contents of 30−70% in mixed Pb-Sn perovskites. In particular, 50% Sn alloyed perovskite with a E_g of 1.25 eV exhibited notably longer carrier lifetimes than all other Sn contents. Importantly, we demonstrate an ideal-E_g (1.33 eV) perovskite composition using the defect-tolerant 50% Sn content ($FA_{0.75}Cs_{0.25}Pb_{0.5}Sn_{0.5}(I_{0.9}Br_{0.1})_3$) with a much-improved carrier lifetime of >1 μs, offering a direction for efficient ideal-bandgap solar cells. Our calculations also indicate the potential of alloying alkaline earth metals for improving the PV performance of Pb-Sn perovskites. This work reveals a general trend of defect tolerance for B-site alloying in OIHPs: a higher VBM (lower CBM) along with stronger ionic bonding potentially leads to enhanced defect tolerance.

■ ASSOCIATED CONTENT

Supporting Information

The Supporting Information is available free of charge at https://pubs.acs.org/doi/10.1021/acsenergylett.1c02105.

DFT calculation methods (calculation details, mixing thermodynamics, defect thermodynamics); experimental methods (materials preparation, perovskite precursor solution, perovskite film fabrication and characterization); UPS calculations; free energy and enthalpy of mixing; origin of the bandgap bowing; projected band structures; PBE-calculated CTLs of intrinsic defects; CTLs of V_{Sn}; calculated relative reaction energies; calculated Δvalues for V_I^-; CTLs of V_I in different doping concentrations; local atomic structures of V_I^- in doped systems; single particle energy levels; PV performance of perovskite solar cells and UV-vis-NIR; and CTLs of I_{int}/Br_{int}, including Figures S1−S12 and Tables S1 and S2 (PDF)

■ AUTHOR INFORMATION

Corresponding Author

Edward H. Sargent − *Department of Electrical and Computer Engineering, University of Toronto, Toronto, Ontario M5S 1A4, Canada;* orcid.org/0000-0003-0396-6495; Email: ted.sargent@utoronto.ca

Authors

Jian Xu − *Department of Electrical and Computer Engineering, University of Toronto, Toronto, Ontario M5S 1A4, Canada;* orcid.org/0000-0002-1532-5145

Aidan Maxwell − *Department of Electrical and Computer Engineering, University of Toronto, Toronto, Ontario M5S 1A4, Canada*

Mingyang Wei − *Department of Electrical and Computer Engineering, University of Toronto, Toronto, Ontario M5S 1A4, Canada*

Zaiwei Wang − *Department of Electrical and Computer Engineering, University of Toronto, Toronto, Ontario M5S 1A4, Canada*

Bin Chen − *Department of Electrical and Computer Engineering, University of Toronto, Toronto, Ontario M5S 1A4, Canada;* orcid.org/0000-0002-2106-7664

Tong Zhu − *Department of Electrical and Computer Engineering, University of Toronto, Toronto, Ontario M5S 1A4, Canada*

Complete contact information is available at: https://pubs.acs.org/10.1021/acsenergylett.1c02105

Author Contributions

†J.X. and A.M. contributed equally to this paper.

Notes

The authors declare no competing financial interest.

■ ACKNOWLEDGMENTS

This research was supported by King Abdullah University of Science and Technology (KAUST) Office of Sponsored Research (OSR) under award no. OSR-2020-CRG9-4350.2. This work was also supported by the U.S. Department of the Navy, Office of Naval Research (N00014-20-1-2572). SciNet is

funded by the Canada Foundation for Innovation under the auspices of Compute Canada.

REFERENCES

(1) NREL. Best Research-Cell Efficiencies, https://www.nrel.gov/pv/cell-efficiency.html (accessed Aug 25, 2021).
(2) Li, H.; Zhang, W. Perovskite Tandem Solar Cells: From Fundamentals to Commercial Deployment. *Chem. Rev.* **2020**, *120* (18), 9835−9950.
(3) Eperon, G. E.; Leijtens, T.; Bush, K. A.; Prasanna, R.; Green, T.; Wang, J. T. W.; McMeekin, D. P.; Volonakis, G.; Milot, R. L.; May, R.; Palmstrom, A.; Slotcavage, D. J.; Belisle, R. A.; Patel, J. B.; Parrott, E. S.; Sutton, R. J.; Ma, W.; Moghadam, F.; Conings, B.; Babayigit, A.; Boyen, H. G.; Bent, S.; Giustino, F.; Herz, L. M.; Johnston, M. B.; McGehee, M. D.; Snaith, H. J. Perovskite-perovskite tandem photovoltaics with optimized band gaps. *Science* **2016**, *354* (6314), 861−865.
(4) Leijtens, T.; Bush, K. A.; Prasanna, R.; McGehee, M. D. Opportunities and challenges for tandem solar cells using metal halide perovskite semiconductors. *Nat. Energy* **2018**, *3* (10), 828−838.
(5) Green, M. A.; Dunlop, E. D.; Hohl-Ebinger, J.; Yoshita, M.; Kopidakis, N.; Hao, X. Solar cell efficiency tables (Version 58). *Prog. Photovoltaics* **2021**, *29* (7), 657−667.
(6) Zhao, D.; Yu, Y.; Wang, C.; Liao, W.; Shrestha, N.; Grice, C. R.; Cimaroli, A. J.; Guan, L.; Ellingson, R. J.; Zhu, K.; Zhao, X.; Xiong, R.-G.; Yan, Y. Low-bandgap mixed tin−lead iodide perovskite absorbers with long carrier lifetimes for all-perovskite tandem solar cells. *Nat. Energy* **2017**, *2* (4), 17018.
(7) Xiao, K.; Lin, R.; Han, Q.; Hou, Y.; Qin, Z.; Nguyen, H. T.; Wen, J.; Wei, M.; Yeddu, V.; Saidaminov, M. I.; Gao, Y.; Luo, X.; Wang, Y.; Gao, H.; Zhang, C.; Xu, J.; Zhu, J.; Sargent, E. H.; Tan, H. All-perovskite tandem solar cells with 24.2% certified efficiency and area over 1 cm^2 using surface-anchoring zwitterionic antioxidant. *Nat. Energy* **2020**, *5*, 870−880.
(8) Tong, J.; Song, Z.; Kim, D. H.; Chen, X.; Chen, C.; Palmstrom, A. F.; Ndione, P. F.; Reese, M. O.; Dunfield, S. P.; Reid, O. G.; Liu, J.; Zhang, F.; Harvey, S. P.; Li, Z.; Christensen, S. T.; Teeter, G.; Zhao, D.; Al-Jassim, M. M.; van Hest, M. F. A. M.; Beard, M. C.; Shaheen, S. E.; Berry, J. J.; Yan, Y.; Zhu, K. Carrier lifetimes of > 1 μs in Sn-Pb perovskites enable efficient all-perovskite tandem solar cells. *Science* **2019**, *364* (6439), 475−479.
(9) Ruhle, S. Tabulated values of the Shockley-Queisser limit for single junction solar cells. *Sol. Energy* **2016**, *130*, 139−147.
(10) Zhou, X.; Zhang, L.; Wang, X.; Liu, C.; Chen, S.; Zhang, M.; Li, X.; Yi, W.; Xu, B. Highly Efficient and Stable GABr-Modified Ideal-Bandgap (1.35 eV) Sn/Pb Perovskite Solar Cells Achieve 20.63% Efficiency with a Record Small Voc Deficit of 0.33 V. *Adv. Mater.* **2020**, *32* (14), e1908107.
(11) Tong, J.; Gong, J.; Hu, M.; Yadavalli, S. K.; Dai, Z.; Zhang, F.; Xiao, C.; Hao, J.; Yang, M.; Anderson, M. A.; Ratcliff, E. L.; Berry, J. J.; Padture, N. P.; Zhou, Y.; Zhu, K. High-performance methylammonium-free ideal-band-gap perovskite solar cells. *Matter* **2021**, *4* (4), 1365−1376.
(12) Klug, M. T.; Milot, R. L.; Patel, J. B.; Green, T.; Sansom, H. C.; Farrar, M. D.; Ramadan, A. J.; Martani, S.; Wang, Z.; Wenger, B.; Ball, J. M.; Langshaw, L.; Petrozza, A.; Johnston, M. B.; Herz, L. M.; Snaith, H. J. Metal composition influences optoelectronic quality in mixed-metal lead−tin triiodide perovskite solar absorbers. *Energy Environ. Sci.* **2020**, *13* (6), 1776−1787.
(13) Leijtens, T.; Prasanna, R.; Gold-Parker, A.; Toney, M. F.; McGehee, M. D. Mechanism of Tin Oxidation and Stabilization by Lead Substitution in Tin Halide Perovskites. *ACS Energy Lett.* **2017**, *2* (9), 2159−2165.
(14) Park, J. S.; Kim, S.; Xie, Z.; Walsh, A. Point defect engineering in thin-film solar cells. *Nat. Rev. Mater.* **2018**, *3* (7), 194−210.
(15) Yin, W.-J.; Shi, T.; Yan, Y. Unusual defect physics in $CH_3NH_3PbI_3$ perovskite solar cell absorber. *Appl. Phys. Lett.* **2014**, *104* (6), 063903.
(16) Shi, T.; Zhang, H.-S.; Meng, W.; Teng, Q.; Liu, M.; Yang, X.; Yan, Y.; Yip, H.-L.; Zhao, Y.-J. Effects of organic cations on the defect physics of tin halide perovskites. *J. Mater. Chem. A* **2017**, *5* (29), 15124−15129.
(17) Agiorgousis, M. L.; Sun, Y. Y.; Zeng, H.; Zhang, S. Strong covalency-induced recombination centers in perovskite solar cell material $CH_3NH_3PbI_3$. *J. Am. Chem. Soc.* **2014**, *136* (41), 14570−14575.
(18) Chung, I.; Song, J. H.; Im, J.; Androulakis, J.; Malliakas, C. D.; Li, H.; Freeman, A. J.; Kenney, J. T.; Kanatzidis, M. G. $CsSnI_3$: Semiconductor or metal? High electrical conductivity and strong near-infrared photoluminescence from a single material. High hole mobility and phase-transitions. *J. Am. Chem. Soc.* **2012**, *134* (20), 8579−8587.
(19) Wang, J.; Li, W.; Yin, W. J. Passivating Detrimental DX Centers in $CH_3NH_3PbI_3$ for Reducing Nonradiative Recombination and Elongating Carrier Lifetime. *Adv. Mater.* **2020**, *32* (6), e1906115.
(20) Meggiolaro, D.; Ricciarelli, D.; Alasmari, A. A.; Alasmary, F. A. S.; De Angelis, F. Tin versus Lead Redox Chemistry Modulates Charge Trapping and Self-Doping in Tin/Lead Iodide Perovskites. *J. Phys. Chem. Lett.* **2020**, *11* (9), 3546−3556.
(21) Ming, W.; Shi, H.; Du, M.-H. Large dielectric constant, high acceptor density, and deep electron traps in perovskite solar cell material $CsGeI_3$. *J. Mater. Chem. A* **2016**, *4* (36), 13852−13858.
(22) Adinolfi, V.; Yuan, M.; Comin, R.; Thibau, E. S.; Shi, D.; Saidaminov, M. I.; Kanjanaboos, P.; Kopilovic, D.; Hoogland, S.; Lu, Z. H.; Bakr, O. M.; Sargent, E. H. The In-Gap Electronic State Spectrum of Methylammonium Lead Iodide Single-Crystal Perovskites. *Adv. Mater.* **2016**, *28* (17), 3406−10.
(23) Heo, S.; Seo, G.; Lee, Y.; Lee, D.; Seol, M.; Lee, J.; Park, J.-B.; Kim, K.; Yun, D.-J.; Kim, Y. S.; Shin, J. K.; Ahn, T. K.; Nazeeruddin, M. K. Deep level trapped defect analysis in $CH_3NH_3PbI_3$ perovskite solar cells by deep level transient spectroscopy. *Energy Environ. Sci.* **2017**, *10* (5), 1128−1133.
(24) Sutter-Fella, C. M.; Miller, D. W.; Ngo, Q. P.; Roe, E. T.; Toma, F. M.; Sharp, I. D.; Lonergan, M. C.; Javey, A. Band Tailing and Deep Defect States in $CH_3NH_3Pb(I_{1-x}Br_x)_3$ Perovskites As Revealed by Sub-Bandgap Photocurrent. *ACS Energy Lett.* **2017**, *2* (3), 709−715.
(25) Meggiolaro, D.; De Angelis, F. First-Principles Modeling of Defects in Lead Halide Perovskites: Best Practices and Open Issues. *ACS Energy Lett.* **2018**, *3* (9), 2206−2222.
(26) Du, M. H. Density Functional Calculations of Native Defects in $CH_3NH_3PbI_3$: Effects of Spin-Orbit Coupling and Self-Interaction Error. *J. Phys. Chem. Lett.* **2015**, *6* (8), 1461−1466.
(27) Zhang, X.; Shen, J. X.; Turiansky, M. E.; Van de Walle, C. G. Minimizing hydrogen vacancies to enable highly efficient hybrid perovskites. *Nat. Mater.* **2021**, *20*, 971−976.
(28) Zhang, X.; Turiansky, M. E.; Shen, J.-X.; Van de Walle, C. G. Iodine interstitials as a cause of nonradiative recombination in hybrid perovskites. *Phys. Rev. B: Condens. Matter Mater. Phys.* **2020**, *101* (14), No. 140101(R).
(29) Li, Z.; Yang, M.; Park, J.-S.; Wei, S.-H.; Berry, J. J.; Zhu, K. Stabilizing Perovskite Structures by Tuning Tolerance Factor: Formation of Formamidinium and Cesium Lead Iodide Solid-State Alloys. *Chem. Mater.* **2016**, *28* (1), 284−292.
(30) Eperon, G. E.; Leijtens, T.; Bush, K. A.; Prasanna, R.; Green, T.; Wang, J. T.-W.; McMeekin, D. P.; Volonakis, G.; Milot, R. L.; May, R.; Palmstrom, A.; Slotcavage, D. J.; Belisle, R. A.; Patel, J. B.; Parrott, E. S.; Sutton, R. J.; Ma, W.; Moghadam, F.; Conings, B.; Babayigit, A.; Boyen, H.-G.; Bent, S.; Giustino, F.; Herz, L. M.; Johnston, M. B.; McGehee, M. D.; Snaith, H. J. Perovskite-perovskite tandem photovoltaics with optimized band gaps. *Science* **2016**, *354* (6314), 861−865.
(31) Meggiolaro, D.; Mosconi, E.; Proppe, A. H.; Quintero-Bermudez, R.; Kelley, S. O.; Sargent, E. H.; De Angelis, F. Energy Level Tuning at the MAPbI3 Perovskite/Contact Interface Using Chemical Treatment. *ACS Energy Lett.* **2019**, *4* (9), 2181−2184.

https://doi.org/10.1021/acsenergylett.1c02105
ACS Energy Lett. 2021, 6, 4220−4227

(32) Huang, Y. T.; Kavanagh, S. R.; Scanlon, D. O.; Walsh, A.; Hoye, R. L. Z. Perovskite-inspired materials for photovoltaics and beyond-from design to devices. *Nanotechnology* **2021**, *32* (13), 132004.
(33) Aziz, A.; Aristidou, N.; Bu, X.; Westbrook, R. J. E.; Haque, S. A.; Islam, M. S. Understanding the Enhanced Stability of Bromide Substitution in Lead Iodide Perovskites. *Chem. Mater.* **2020**, *32* (1), 400−409.
(34) Abdi-Jalebi, M.; Andaji-Garmaroudi, Z.; Cacovich, S.; Stavrakas, C.; Philippe, B.; Richter, J. M.; Alsari, M.; Booker, E. P.; Hutter, E. M.; Pearson, A. J.; Lilliu, S.; Savenije, T. J.; Rensmo, H.; Divitini, G.; Ducati, C.; Friend, R. H.; Stranks, S. D. Maximizing and stabilizing luminescence from halide perovskites with potassium passivation. *Nature* **2018**, *555* (7697), 497−501.
(35) Chadi, D. J.; Chang, K. J. Energetics of DX-center formation in GaAs and $Al_xGa_{1-x}As$ alloys. *Phys. Rev. B: Condens. Matter Mater. Phys.* **1989**, *39* (14), 10063−10074.
(36) Van de Walle, C. G. DX-center formation in wurtzite and zinc-blende $Al_xGa_{1-x}N$. *Phys. Rev. B: Condens. Matter Mater. Phys.* **1998**, *57* (4), R2033−R2036.
(37) Lany, S.; Zunger, A. Intrinsic DX Centers in Ternary Chalcopyrite Semiconductors. *Phys. Rev. Lett.* **2008**, *100* (1), 016401.
(38) Savill, K. J.; Ulatowski, A. M.; Herz, L. M. Optoelectronic Properties of Tin-Lead Halide Perovskites. *ACS Energy Lett.* **2021**, *6* (7), 2413−2426.
(39) Phung, N.; Felix, R.; Meggiolaro, D.; Al-Ashouri, A.; Sousa e Silva, G.; Hartmann, C.; Hidalgo, J.; Kobler, H.; Mosconi, E.; Lai, B.; Gunder, R.; Li, M.; Wang, K.-L.; Wang, Z.-K.; Nie, K.; Handick, E.; Wilks, R. G.; Marquez, J. A.; Rech, B.; Unold, T.; Correa-Baena, J.-P.; Albrecht, S.; De Angelis, F.; Bar, M.; Abate, A. The Doping Mechanism of Halide Perovskite Unveiled by Alkaline Earth Metals. *J. Am. Chem. Soc.* **2020**, *142* (5), 2364−2374.
(40) Pérez-del-Rey, D.; Forgács, D.; Hutter, E. M.; Savenije, T. J.; Nordlund, D.; Schulz, P.; Berry, J. J.; Sessolo, M.; Bolink, H. J. Strontium Insertion in Methylammonium Lead Iodide: Long Charge Carrier Lifetime and High Fill-Factor Solar Cells. *Adv. Mater.* **2016**, *28* (44), 9839−9845.
(41) Lany, S.; Zunger, A. Comment on "Intrinsic n-type behavior in transparent conducting oxides: a comparative hybrid-functional study of In_2O_3, SnO_2, and ZnO". *Phys. Rev. Lett.* **2011**, *106* (6), 069601.
(42) Buckeridge, J.; Catlow, C. R. A.; Farrow, M. R.; Logsdail, A. J.; Scanlon, D. O.; Keal, T. W.; Sherwood, P.; Woodley, S. M.; Sokol, A. A.; Walsh, A. Deep vs shallow nature of oxygen vacancies and consequentn-type carrier concentrations in transparent conducting oxides. *Phys. Rev. Mater.* **2018**, *2* (5), 054604.
(43) Chatratin, I.; Sabino, F. P.; Reunchan, P.; Limpijumnong, S.; Varley, J. B.; Van de Walle, C. G.; Janotti, A. Role of point defects in the electrical and optical properties of In_2O_3. *Phys. Rev. Mater.* **2019**, *3* (7), 074604.
(44) Janotti, A.; Van de Walle, C. G. Oxygen vacancies in ZnO. *Appl. Phys. Lett.* **2005**, *87* (12), 122102.

https://doi.org/10.1021/acsenergylett.1c02105
ACS Energy Lett. 2021, 6, 4220−4227